# Document made available under the Patent Cooperation Treaty (PCT)

International application number: PCT/US04/033581

International filing date: 12 October 2004 (12.10.2004)

Document type: Certified copy of priority document

Document details: Country/Office: US
Number: 60/555,590
Filing date: 22 March 2004 (22.03.2004)

Date of receipt at the International Bureau: 04 July 2005 (04.07.2005)

Remark: Priority document submitted or transmitted to the International Bureau in compliance with Rule 17.1(a) or (b)

World Intellectual Property Organization (WIPO) - Geneva, Switzerland
Organisation Mondiale de la Propriété Intellectuelle (OMPI) - Genève, Suisse

1336301

# UNITED STATES OF AMERICA

## TO ALL TO WHOM THESE PRESENTS SHALL COME:

**UNITED STATES DEPARTMENT OF COMMERCE**

**United States Patent and Trademark Office**

***June 21, 2005***

**THIS IS TO CERTIFY THAT ANNEXED HERETO IS A TRUE COPY FROM THE RECORDS OF THE UNITED STATES PATENT AND TRADEMARK OFFICE OF THOSE PAPERS OF THE BELOW IDENTIFIED PATENT APPLICATION THAT MET THE REQUIREMENTS TO BE GRANTED A FILING DATE.**

**APPLICATION NUMBER:** ***60/555,590***
**FILING DATE:** ***March 22, 2004***
**RELATED PCT APPLICATION NUMBER:** ***PCT/US04/33581***

**Certified by**

**Under Secretary of Commerce**
**for Intellectual Property**
**and Director of the United States**
**Patent and Trademark Office**

PTO/SB/16 (01-04)
Approved for use through 07/31/2006. OMB 0651-0032
U.S. Patent and Trademark Office; U.S. DEPARTMENT OF COMMERCE


# PROVISIONAL APPLICATION FOR PATENT COVER SHEET

This is a request for filing a PROVISIONAL APPLICATION FOR PATENT under 37 CFR 1.53(c).

Express Mail Label No. EV240599248US



| INVENTOR(S) | | |
|---|---|---|
| Given Name (first and middle [if any]) | Family Name or Surname | Residence (City and either State or Foreign Country) |
| Yadong<br>A. Paul | Yin<br>Alivisatos | Berkeley, CA<br>Berkeley, CA |

*Additional inventors are being named on the* _____ *separately numbered sheets attached hereto*

**TITLE OF THE INVENTION (500 characters max)**

Formation of Hollow Nanocrystals

*Direct all correspondence to:* **CORRESPONDENCE ADDRESS**

☒ Customer Number: 08076

*OR*

| | | | | | |
|---|---|---|---|---|---|
| ☐ Firm or Individual Name | | | | | |
| Address | | | | | |
| Address | | | | | |
| City | | State | | Zip | |
| Country | | Telephone | | Fax | |

**ENCLOSED APPLICATION PARTS** ***(check all that apply)***

☒ Specification *Number of Pages* 14 ☐ CD(s), Number _____

☒ Drawing(s) *Number of Sheets* 4 ☒ Other (specify) Postcard

☐ Application Data Sheet. See 37 CFR 1.76

**METHOD OF PAYMENT OF FILING FEES FOR THIS PROVISIONAL APPLICATION FOR PATENT**

☒ Applicant claims small entity status. See 37 CFR 1.27.

☐ A check or money order is enclosed to cover the filing fees.

☒ The Director is hereby authorized to charge filing fees or credit any overpayment to Deposit Account Number: 12-0690

☐ Payment by credit card. Form PTO-2038 is attached.

**FILING FEE Amount ($)**

80.00

The invention was made by an agency of the United States Government or under a contract with an agency of the United States Government.

☐ No.

☒ Yes, the name of the U.S. Government agency and the Government contract number are: U.S. Department of Energy, Prime Contract No. DE-AC03-76SF00098



*Respectfully submitted,*

SIGNATURE C R Nold

TYPED or PRINTED NAME Charles R. Nold

TELEPHONE 510-486-6503

Date 3/22/04

REGISTRATION NO. 46,470 *(If appropriate)*

Docket Number: IB-2012P

***USE ONLY FOR FILING A PROVISIONAL APPLICATION FOR PATENT***

3/20/04

FILE

IB-2012P

# Formation of Hollow Nanocrystals [redacted]

Yadong Yin, [redacted], A. Paul Alivisatos*

Department of Chemistry, University of California at Berkeley, and Materials Science Division, Lawrence Berkeley National Laboratory, Berkeley, CA 94720, USA.

*To whom correspondence should be addressed. Email: alivis@uclink4.berkeley.edu

**Abstract**

We demonstrate that hollow nanocrystals can be synthesized through a mechanism analogous to the Kirkendall Effect, in which pores form due to the difference in diffusion rates between two components in a diffusion couple. Starting with cobalt nanocrystals, we show that their reaction in solution with oxygen, and sulfur or selenium leads to the formation of hollow nanocrystals of the resulting oxide and chalcogenides. This process provides a general route to the synthesis of hollow nanostructures of a large number of compounds. A simple extension of the process yields platinum-cobalt oxide yolk-shell nanostructures which may serve as nanoscale reactors in catalytic applications.

Porous solid materials are important in many areas of modern science and technology, including ion exchange, molecular separation, catalysis, chromatography, microelectronics, and energy storage (1-3). Notable examples are microporous (< 2 nm) zeolites and mesoporous (2-50 nm) silicate and carbonaceous materials. The ability to manipulate the structure and morphology of porous solids on a nanometer scale would enable greater control of local chemical environment (4-6). We demonstrate that nanoscale pores can develop inside nanocrystals with a mechanism analogous to void formation in the Kirkendall Effect, where the mutual diffusion rates of two components in a diffusion couple differ by a considerable amount (7). We choose cobalt nanocrystals as a starting material to show that hollow nanocrystals of cobalt oxide and chalcogenides can be successfully synthesized by reacting cobalt colloidal solution with oxygen, and sulfur or selenium.

It has been known for over half a century that porosity may result from differential solid-state diffusion rates of the reactants in an alloying or oxidation reaction. In 1947, Smigelkas and Kirkendall reported the movement of the interface between a diffusion couple, i.e., copper and zinc in brass, as the result of the different diffusion rates of these two species at an elevated temperature (7). This phenomenon, now called the Kirkendall Effect, was the first experimental proof that atomic diffusion occurs through vacancy exchange, and not by the direct interchange of atoms. The net directional flow of matter is balanced by an opposite flow of vacancies, which can condense into pores or annihilate at dislocations. Directional material flows also result from coupled reaction-diffusion phenomena at a solid/gas or solid/liquid interface, leading to deformation and/or void formation during the growth of metal oxide or sulfide films (8, 9). These voids are usually explained by outward transport of fast-moving cations through the oxide layer and a balancing inward flow of vacancies to the vicinity of the metal-oxide interface.

Interface motion and the formation of pores have been studied due to their impact on the reproducibility and reliability of solders, passivation layers, diffusion barriers etc., but not generally as a method of preparing porous materials. The pores produced at a metal-metal diffusion couple or near the metal-oxide interface of a growing oxide do not yield monodisperse, ordered arrays but form a very heterogeneous ensemble. Also, the observed volume fraction for pores is commonly much smaller than would be expected for the known material flows. These observations are a direct result of the large volume of material that vacancies can diffuse into and the large number of defects they can react with (10).

If the faster-diffusing species is confined into a nanocrystal 'core', the net rate of vacancy injection should increase dramatically due to the high surface-to-volume ratio of the particle and the absence of defects in the core. Within the small volume of a transforming nanocrystal, the supersaturated vacancy cloud is likely to coalesce into a single void. Previous studies on the interdiffusion of 30-micrometer powders with layered composition showed significant porosity, but the geometry and distribution of the pores were not uniform, probably due to aggregation and bulk-like dimension of the particles (11). Significant progress has recently been made in synthesizing colloidal nanocrystals with well-controlled size, shape and surface properties (12-14). Employing such high-quality nanocrystals as the starting materials, it should be possible to produce a relatively uniform population of hollow nanostructures.

We have chosen cobalt nanocrystals as the main starting material. A number of chemical methods have been developed to synthesize uniform cobalt nanocrystals in solution (12, 15). Furthermore, cobalt reacts readily with other species such as sulfur and oxygen. Since cobalt is the major component in one class of superalloys, its high-temperature oxidation and sulfidation have been well studied (16, 17). It is known that oxidation and sulfidation of bulk cobalt under

vapor at high temperature is mainly controlled by outward diffusion of cobalt cations (18). This mode of growth operating on nanocrystals is expected to lead to hollow structures.

Sulfidation of cobalt was the first case where we observed hollow nanostructures. Cobalt sulfide hollow nanospheres are synthesized in one pot by immediate injection of a solution of sulfur in *o*-dichlorobenzene into a hot cobalt nanocrystal dispersion (as shown in the transmission electron microscopy (TEM) image in Fig. 1A) that is prepared by literature methods (15, 19). At 445 K, the reaction between cobalt and sulfur completes within a few seconds, resulting in a black solution of cobalt sulfide nanocrystals. We have confirmed that hollow particles are produced at temperatures as low as 373 K. The hollow particles are very stable in solution suggesting that the chemical transformation of the surface does not disrupt the coating of the nanocrystals by surfactant molecules. Upon washing with methanol, the surfactant layer is removed and it is no longer possible to redissolve the precipitate in *o*-dichlorobenzene.

Outward flow of cobalt through the sulfide shell results in supersaturation of vacancies, which condense to form a single hole in each nanoparticle (Figs. 1B-D). Two stable cobalt sulfide phases are observed, linnaeite ($Co_3S_4$) and cobalt pentlandite ($Co_9S_8$), depending on the sulfur-to-cobalt molar ratio used in the synthesis. X-ray powder diffraction (XRD) patterns in Fig. 1E show the evolution of the crystal structure as the molar ratio of sulfur to cobalt is increased. $Co_9S_8$ is the only sulfide phase observed when the molar ratio is lower than 9:8, while $Co_3S_4$ also appears in the patterns when the molar ratio slightly exceeds this value. Only $Co_3S_4$ is obtained when the molar ratio of sulfur to cobalt is above 3:4. The size distribution of the sulfide hollow particles is similar to the starting cobalt nanocrystals. Monodisperse hollow nanocrystals self-assemble into ordered hexagonal arrangements when evaporated slowly on the surface of a carbon coated TEM grid. The assembly process is driven by surface tension and van der Waals

forces. Cobalt sulfide nanocrystals do not form superlattices as readily as cobalt nanocrystals do, probably due to a diminished van der Waals force (19). Assemblies of hollow nanoparticles present a distinct topology of ordered porous materials. In terms of the accessibility of pores from the outside, they fall between mesoporous materials with accessible channels and void lattices where pores are confined in a continuous matrix (20).

Kinematical diffraction simulations indicate that the XRD peaks are too broad to be consistent with a single crystal shell of dimensions observed by TEM (21). A satisfactory fit to the data in Fig. 1E(d) is obtained by assuming a 4.5 nm cubic crystalline domain. TEM micrographs (Fig. 1D) of the same sample show that the average outer diameter of the hollow $Co_9S_8$ nanocrystals is around 15 nm. A reasonable explanation is that the shell of each hollow sphere is multi-crystalline. This is confirmed by high resolution transmission electron microscopy (HRTEM), which shows that both $Co_9S_8$ and $Co_3S_4$ hollow nanocrystals are composed of multiple crystallographic domains (Fig. 1C). The arrangement of the domains is analogous to the columnar morphology of grains often observed in thin film growth. The multi-crystalline structure implies possible applications of these hollow nanocrystals as nanoscale reactors since small molecules may be able to penetrate the shell through the grain boundaries.

In all instances of sulfidation, we have found that the diameter of the hole in the center of the nanocrystals is 40-70% of the initial particle size (starting with cobalt particles with a size distribution of 7%, a single synthesis yields a hole size distribution of 13%). If sulfur transport through the growing shell is negligible, as shown for bulk sulfidation by marker experiments (18), then the two diameters are expected to be identical. Significant inward sulfur transport could occur through grain boundaries or during the formation of the first few monolayers of sulfide. It is also possible that inward relaxation of the hole occurs, due to annihilation of vacancies at a

semicoherent or incoherent cobalt-sulfide interface. Finally, the estimation of the hole size by visual inspection of TEM images may produce systematic errors. We attempted to examine the possibility of inward sulfur transport by performing the $Co_3S_4$ synthesis at different sulfur concentrations. Increased sulfur concentration increases hole size and enhances outward growth of the shell, indicating that cobalt mobility rather than sulfur mobility is affected. This finding is consistent with bulk sulfidation studies (18), where it is observed that an increased sulfur vapor pressure leads to injection of more cation vacancies into the growing sulfide and enhances the parabolic rate constant for sulfide growth.

For bulk cobalt, the rates of oxidation are 3-4 orders of magnitude lower than those of sulfidation above 750 K (18). This is also true under the conditions we use to produce hollow nanocrystals, and oxidation of nanocrystals takes about three hours at 455 K. Fig. 2(A-D) shows the evolution of the morphology of the nanocrystals with time as an $O_2$/Ar mixture is flowed through the cobalt colloidal solution. The XRD shows the presence of metallic cobalt up to 30 minutes (Fig. 2E). The solution of particles still displays weak ferrofluidic response to a 1T magnet at that point, suggesting that small cobalt cores remain. It takes about three hours for the cobalt cores to be completely consumed: central pores are clearly distinguishable for all nanocrystals under TEM and the solution shows no magnetic response.

The evolution of hollow morphology is best illustrated by following the reaction of cobalt nanocrystals with selenium. In bulk systems, annihilation of excess vacancies at dislocations and boundaries can produce stresses leading to the formation of cracks near the interface; the cracks then act as nuclei for the further condensation of supersaturated vacancies (11). While the exact mechanism is likely to be different, in nanocrystals voids also begin to develop and merge at the boundary (Fig. 3). The high defect content and surface energy associated with the boundary

favors the nucleation of voids there. Also, as vacancies diffuse inwards, they will be more concentrated at the boundary rather than in the interior of the core. As the reaction proceeds in time, more cobalt atoms diffuse out to the shell and the accompanying transport of vacancies leads to growth and merging of the initial voids. This results in the formation of bridges of material between the core and the shell that persist until the core is completely consumed. These bridges provide a fast transport path for outward diffusion of cobalt atoms which can then spread on the inner shell surface. A similar phenomenon was observed for bulk powders (11). We note that the growth rate of pores drops dramatically when the cobalt cores become relatively small. Most of the pore volume seems to form during the first few minutes, while it takes about 30 minutes for the cobalt cores to completely disappear. This may be due to the fact that as the bridges are also consumed during the reaction, a smaller cross-sectional area is available for solid-state transport of materials.

As an illustration of the generality of the ideas presented here, we have synthesized several other hollow nanostructures. Sulfidation of disk-shaped cobalt nanocrystals (21) was observed to result in the formation of hollow nanodisks with cylindrical pores, indicating that spherical symmetry is not required for obtaining shells of regular thickness. Preliminary studies on oxidation of iron nanospheres and sulfidation of cadmium nanospheres also resulted in hollow structures, thus validating our approach for metallic cores in general. Theoretically, the mobilities of the reacting species do not have to be drastically different to result in vacancy transport. Placing solid nanocrystals containing one reactant in a comparatively dilute solution creates an additional asymmetry that may favor the creation of hollow structures: the relatively large change in the concentration of the core material between the core and the solution provides a greater driving force for the outward diffusion of the core material. Thus, numerous

combinations of reactants may be expected to produce various hollow nanostructures of insulators, semiconductors and even metals. A recent report on the formation of gold nanoboxes may involve the same mechanism at some stage, although the dimension of the structures produced is an order of magnitude larger (22).

Hollow nanocrystals offer exciting possibilities in material design for applications in catalysis, nanoelectronics, nano-optics, drug delivery systems, and as building blocks for light-weight structural materials (23-25). For example, accurate fixation of the catalyst within the pores, combined with other emerging techniques of chemical control (26), could result in better reaction control and new products. To demonstrate the use of hollow nanocrystals in catalysis, we study their function as nanoreactors each containing one noble metal nanocrystal. A Pt@CoO yolk-shell nanostructure is synthesized, in which a platinum nanocrystal of a few nanometers is encapsulated in a CoO shell. Three steps are involved in the preparation of these nanoreactors: synthesis of platinum seeds by a modified "polyol" process (27), deposition of cobalt on platinum to form Pt@Co core-shell nanocrystals, and transformation of cobalt into CoO hollow structures (28). Fig. 4A shows a typical sample of platinum particles with an average diameter around 3 nm. The deposition of cobalt onto platinum at the reaction temperature yields no alloy, only Pt core/Co shell particles, as confirmed by XRD analyses. The oxidation reaction removes cobalt atoms away from the platinum particle surface, leading to the formation of a Pt yolk/CoO shell structure (Fig. 4B). No free platinum particles were found by TEM inspection of the Pt@CoO sample. The size of Pt@CoO particles can be controlled by changing the diameter and number of the platinum seeds, and the amount of cobalt carbonyl precursor.

In order to determine if the Pt@CoO materials were active as heterogeneous catalysts, the hydrogenation of ethylene was chosen as a model reaction since it readily occurs at ambient

conditions on many transition metal catalysts. Platinum is one of the most active metals for this reaction while the activity of metallic cobalt is approximately two orders of magnitude lower (29). We found that pure CoO hollow nanocrystals are inactive for ethylene hydrogenation (30), even following a 1 h $H_2$ pre-reduction at 373 K. Only upon reduction at 473 K for 1 h is ethane detected at temperatures >300 K. Samples containing platinum without pretreatment are active for $C_2H_4$ hydrogenation at temperatures as low as 208 K. The steady state turnover frequency for ethane formation at 227 K is $8.3\times10^{-3}$ $s^{-1}$ (31), which is comparable to the rate of $3.5 \times 10^{-2}$ $s^{-1}$ measured on a 0.04% $Pt/SiO_2$ catalyst (32), and $1.7 \times 10^{-2}$ $s^{-1}$ measured on pure platinum powders (0.2 - 1.6 μm). These observations indicate that the reaction is catalyzed by platinum particles, not the CoO shell. This also confirms that a route exists for ethylene and hydrogen entry into the CoO shell interior. The grain boundaries on the shell are the most probable entry points for ethylene and hydrogen diffusion into as well as ethane diffusion out of the shell. Comparing to catalysts supported on other mesoporous materials, isolation of catalyst nanoparticles within solid shells should minimize secondary reaction of the products that degrade selectivity and product distribution. Furthermore, any synergistic interactions between catalyst and support can be more efficiently utilized when each catalyst particle is in contact with a shell of the support material.

All references are hereby incorporated by reference in their entirety.

References:

1. D. Zhao, P. Yang, Q. Huo, B. F. Chmelka, G. D. Stucky, *Curr. Opin. Solid State Mater. Sci.* **3**, 111 (1998).

2. S. A. Johnson, P. J. Ollivier, T. E. Mallouk, *Science* **283**, 963 (1999).

3. A.-P. Li, F. Müller, A. Birner, K. Nielsch, U. Gösele, *Adv. Mater.* **11**, 483 (1999).

4. D. Trong On, D. Desplantier-Giscard, C. Danumah, S. Kaliaguine, *Appl. Catal.* **222**, 299 (2001).

5. M. E. Davis, *Nature* **417**, 813 (2002).

6. W. Gu, M. Warrier, V. Ramamurthy, R. G. Weiss, *J. Am. Chem. Soc.* **121**, 9467 (1999).

7. A. D. Smigelskas, E. O. Kirkendall, *Trans. AIME* **171**, 130 (1947).

8. C. E. Birchenall, *J. Electrochem. Soc.* **103**, 619 (1956).

9. J. C. Colson, M. Lambertin, P. Barret in *Proc. 7th Int. Symp. Reactivity of Solids*, J. S. Anderson, F. S. Stone, M. W. Roberts Eds. (Chapman and Hall, London, 1972), pp. 283-293.

10. G. B. Gibbs, *Oxid. Met.* **16**, 147 (1981).

11. F. Aldinger, *Acta Met.* **22**, 923 (1974).

12. C. B. Murray, C. R. Kagan, M. G. Bawendi, *Annu. Rev. Mater. Sci.* **30**, 545 (2000).

13 X. Peng et al., *Nature* **404**, 59 (2000)

14. R. Jin et al., *Nature* **425**, 487 (2003).

15. V. F. Puntes, K. M. Krishnan, A. P. Alivisatos, *Science* **291**, 2115 (2001).

16. S. Mrowec, K. Przybylski, *Oxid. Met.* **11**, 365 (1977).

17. A. Devin, *Cobalt* **30**, 19 (1966).

18. S. Mrowec, M. Danlelewski, A. Wojtowicz, *J. Mater. Sci.* **33**, 2617 (1998).

19. V. F. Puntes, K. M. Krishnan, P. Alivisatos, *Appl. Phys. Lett.* **78**, 2187 (2001).

20. N. M. Ghoniem, D. Walgraef, S. J. Zinkle, *J. Comput. Aided Mater. Des.* **8**, 1 (2001).

21. V. F. Puntes, D. Zanchet, C. K. Erdonmez, A. P. Alivisatos, *J. Am. Chem. Soc.* **124**, 12874 (2002).

22. Y. Sun, Y. Xia, *Science* **298**, 2176 (2002).

23. F. Caruso, R. A. Caruso, H. Möhwald, *Science* **282**, 1111 (1998).

24. U. S. Schwarz, S. A. Safran, *Phys. Rev. E* **62**, 6957 (2000).

25. W. S. Sanders, L. J. Gibson, *Mater. Sci. Eng. A* **352**, 150 (2003).

26. N. J. Turro, *Acc. Chem. Res.* **33**, 637 (2000).

27. N. S. Sobal, U. Ebels, H. Möhwald, M. Giersig, *J. Phys. Chem.* **107**, 7351 (2003).

28. Platinum acetylacetonate is reduced with a long-chain polyol to form uniform platinum nanoparticles in the presence of surfactants such as oleic acid, oleylamine, and trioctylphosphine. The size of the platinum particles can be tuned from 1 to 10 nm, depending on the concentration of surfactants. $Co_2(CO)_8$ is then injected into the hot solution and decomposed to form a conformal coating on platinum nanocrystals. Oxidation of the Pt@Co nanocrystals is performed a few minutes after the introduction of cobalt carbonyl by blowing a stream of $O_2$/Ar (1:4 in volume ratio, 120 ml/min) mixture into the colloidal solution at 455 K. The system is kept under stirring for 3 hours. A black stable colloidal dispersion in *o*-dichlorobenzene is obtained. Finally, the Pt@CoO particles are precipitated by methanol, washed with toluene and methanol three times, and dried under vacuum. Typical nitrogen adsorption/desorption measurement on the powder at 77K shows a type IV isotherm with type H2 hysteresis, with a Brunauer-Emmet-Teller (BET) surface area of 65 $m^2/g$ and a total pore volume of 0.0676 $cm^3/g$.

29. G. A. Somorjai, *Introduction to Surface Chemistry and Catalysis*. (John Wiley and Sons, Inc., New York, 1994).

30. The hydrogenation of ethylene is studied at atmospheric pressure in a differentially operated plug flow reactor. Standard conditions are 11 Torr $C_2H_4$, 150 Torr $H_2$, and 208-353K (sample dependent).

31. Rates were measured on a per gram basis. They were normalized per mole of surface platinum species ($Pt_s$) to obtain a turnover frequency (molecule $Pt_s^{-1}s^{-1}$). Moles of $Pt_s$ was

determined by D=1.13/d where D is the platinum dispersion (ratio of $Pt_s$ to the total platinum content ($Pt_t$)) and d is the particle size in nm. The platinum particle size was determined from number average TEM measurements.

32. R. D. Cortright, S. A. Goddard, J. E. Rekoske, J. E. Dumesic, *J. Catal.* **127**, 342 (1991).

33. This work was supported by the Air Force Office of Scientific Research under award number F49620-01-1-0033, and by the Director, Office of Energy Research, Office of Science, Division of Materials Sciences, of the U.S. Department of Energy under Contract No. DE-AC03-76SF00098. Y.Y. thanks Prof. J. Fréchet for the valuable discussions. R.M.R. would like to acknowledge the Ford Motor Company and the Berkeley Catalysis Center for financial support.

## Captions to Figures

Fig. 1. (A) TEM image of cobalt nanocrystals synthesized by injecting 0.54 g of $Co_2(CO)_8$ in 3 ml of *o*-dichlorobenzene into 0.1 ml of oleic acid and 0.1 g of trioctylphosphine oxide in 15 ml of *o*-dichlorobenzene at 455 K. (B, D) TEM images of the cobalt sulfide phases synthesized by injecting sulfur in *o*-dichlorobenzene (5 ml) into cobalt nanocrystal solution with different Co/S molar ratios: (B) $Co_3S_4$ with Co:S=9:12 and (D) $Co_9S_8$ with Co:S=9:8. The $Co_3S_4$ particles were synthesized from the cobalt sample shown in (A), while the $Co_9S_8$ particles started from another cobalt sample which has an average diameter around 11 nm. (C) HRTEM images of $Co_3S_4$ (left) and $Co_9S_8$ (right). (E) XRD patterns of cobalt nanocrystals (a) and cobalt sulfide synthesized with different Co/S molar ratios: (b) 9:5; (c) 9:7; (d) 9:8; (e) 9:10; (f) 9:11; (g) 9:12; and (h) 9:18.

Fig. 2. Evolution of CoO hollow nanocrystals with time by blowing a stream of $O_2$/Ar (1:4 in volume ratio, 120 ml/min) mixture through a cobalt colloidal solution at 455 K. (A-D) TEM images of the solutions after flowing $O_2$/Ar for (A) 0 min; (B) 30 min; (C) 80 min; (D) 210 min. The inset shows a HRTEM of a CoO hollow nanocrystal. (E) XRD patterns of the sample obtained from the solution after flow $O_2$/Ar for (a) 0 min; (b) 2.5 min; (c) 5.5 min; (d) 10 min; (e) 30 min; (f) 80 min; and (g) 210 min.

Fig. 3. Evolution of CoSe hollow nanocrystals with time by injection of a suspension of selenium in *o*-dichlorobenzene into a cobalt nanocrystal solution at 455 K, from top-left to bottom-right: 0 sec, 10 sec, 20 sec, 1 min, 2 min and 30 min. The Co/Se molar ratio is 1:1.

Fig. 4. (A) Platinum nanocrystals prepared by injecting a solution of 0.15 g platinum acetylacetonate in 5 ml *o*-dichlorobenzene into a refluxing bath of 10 ml *o*-dichlorobenzene containing 0.3 g of 1,2-hexadecanediol, 0.1 ml of oleic acid, 0.1 ml of oleylamine and 0.06 ml of trioctylphosphine. The solution was then heated for another 120 minutes. (B) Pt@CoO yolk-shell nanostructures formed by injecting 1.08 g $Co_2(CO)_8$ in 6 ml *o*-dichlorobenzene into the platinum nanocrystals solution, and followed by the oxidation of the product particles by blowing a stream of $O_2$/Ar (1:4 in volume ratio, 120 ml/min) mixture into the colloidal solution at 455 K. The system was kept at the same temperature under stirring for 3 hours.

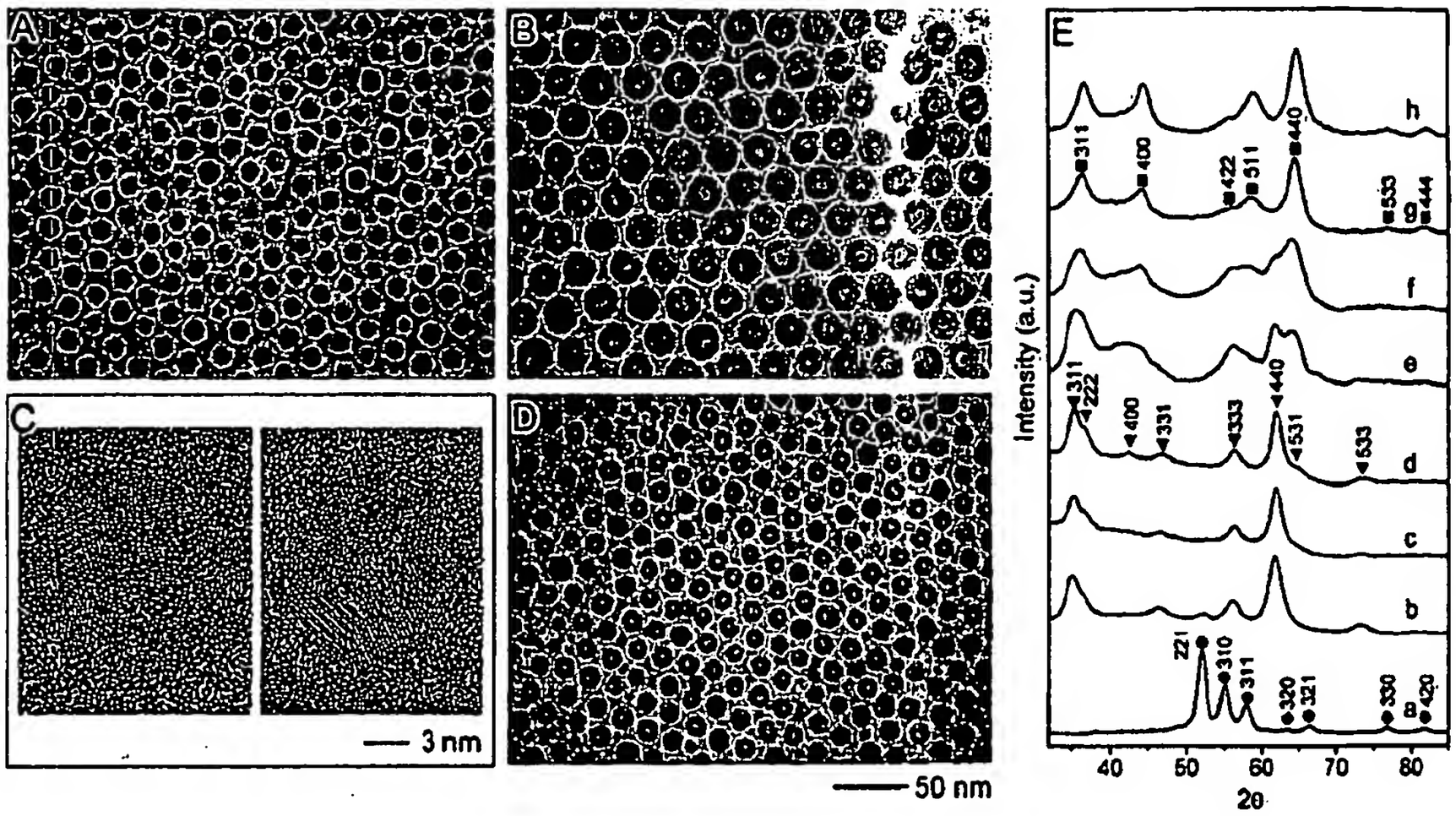


**Alivisatos_Fig. 1**

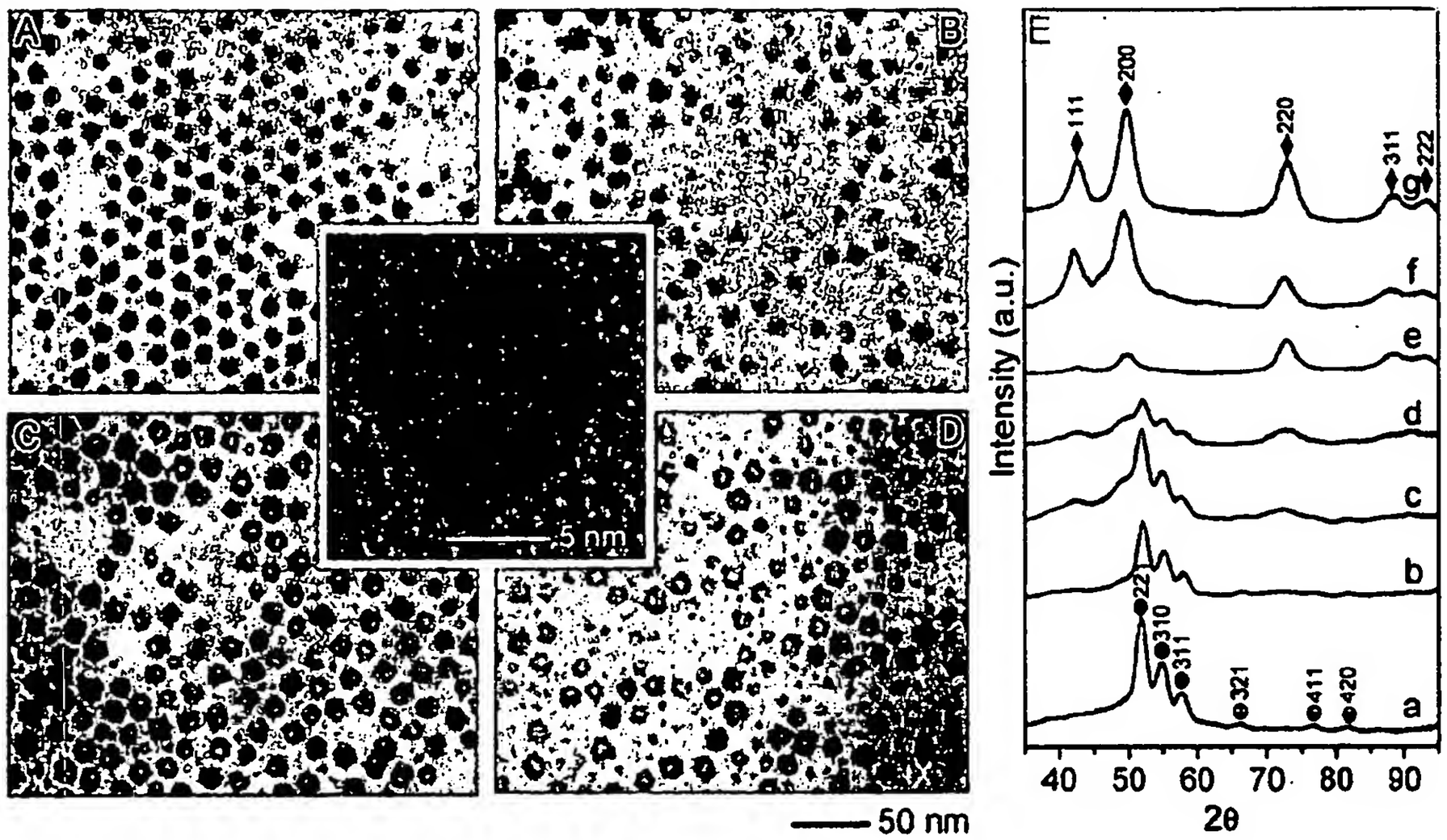


**Alivisatos_Fig. 2**

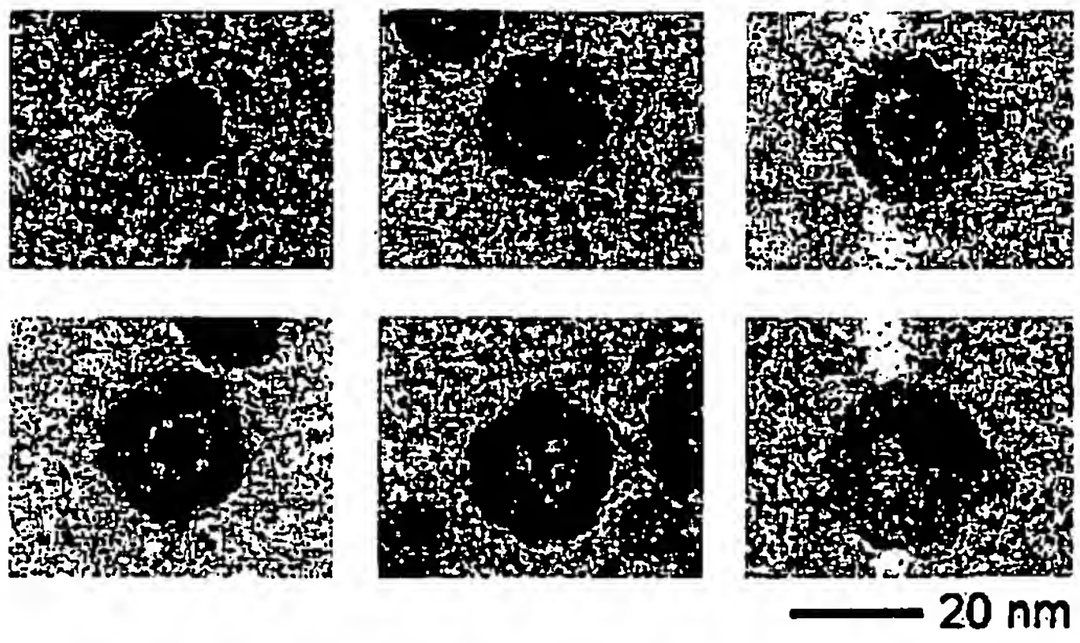


**Alivisatos_Fig. 3**

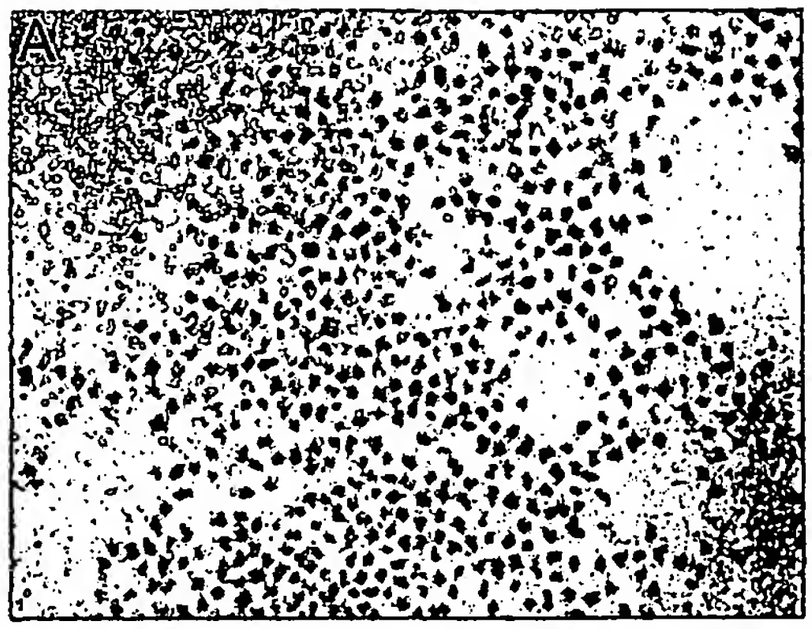


Alivisatos_Fig. 4



4/4